Tight Binding Descriptions of Graphene and Its Derivatives

A Thesis Presented to the Department of

THEORETICAL AND APPLIED PHYSICS

African University of Science and Technology

In Partial Fulfillment of the Requirements for the Degree of

MASTER OF SCIENCE

BY

ISAH MUHAMMAD MAIKUDI

December 2017

Certification

This is to certify that the thesis titled "TIGHT BINDING DESCRIPTIONS OF GRAPHENE AND ITS DERIVATIVES" submitted to the school of postgraduate studies, African University of Science and Technology (AUST), Abuja, Nigeria for the award of the Master's degree is a record of original research carried out by Isah Muhammad Maikudi in the Department of Theoretical and applied physics.

TIGHT BINDING DESCRIPTIONS OF GRAPHENE AND IT IS DERIVATIVES

BY

Isah Muhammad Maikudi

A THESIS APPROVED BY THE THEORETICAL AND APPLIED PHYSICS DEPARTMENT

RECOMMENDED:

.....
Supervisor: Dr. Emine Kucukbenli

.....
Dr. Omololu Akin-Ojo

.....
Head, Department of Theoretical Physics

APPROVED:

.....
Chief Academic Officer (Prof. C. E. Chidume)

.....
Date

Abstract

Graphene is an effectively two dimensional form of carbon atoms arranged in honeycomb lattice. Due to its lightweight, high electron mobility and other special electronic properties it is considered both an academically interesting and industrially promising candidate for various electronics applications. Many investigations focused on graphene require theoretical simulations to be performed over a large number of unit cells of graphene. For simulation scenarios where *ab-initio* methods are computationally too costly, researchers often refer to the low-cost but still highly accurate tight-binding (TB) model. In TB model, the electron interaction is parametrized, either through the derivation of parameters using first principles methods, or by fitting to experimental results. The results of TB simulations depend strongly on this parameterization, therefore it is very important to know the level of accuracy and transferability of these parameters. In this research project we will simulate the band structure and density of states of graphene and other derivative of carbon structures such as nanoribbons using a state-of-the-art parameter set; and compare their performance to the results of ab initio calculations. The resulting comparison will serve as a benchmark for future studies on graphene and derivatives.

Contents

1 Introduction **1**

2 Linear Combination of Atomic Orbitals **3**
2.1 H-like atom and atomic orbitals 3
2.1.1 Asymptotic analysis 4
2.2 Linear Combination: H_2 dimer 6
2.3 Linear Combination: H trimer 8

3 Tight Binding Approximation **10**
3.1 H chain and Born-von Karman boundary conditions 10
3.2 Bloch Theorem 12
3.3 Tight binding model for graphene 13

4 Density functional theory **16**
4.1 Formalism 16
4.2 Pseudopotentials 19

5 Graphene **21**
5.1 Tight Binding Results 22
5.1.1 Ab-initio result 28

6 Nanoribbons **31**
6.1 Results for Zigzag Ribbon (zGNR) 31
6.2 Results for Armchair Ribbon (aGNR) 33

7 Conclusion and Outlook **35**

List of Figures

1.1 All dimensionalities of Carbon 2

5.1 (a): Graphene with its sub-lattices. (b): The first brilloune zone and the IBZ 22
5.2 PythTB calculations of Graphene, t_0 values used are 2.74eV(top), 2.80eV(mid), 3.00eV(bottom panel). 24
5.3 second nearest with, $t_o = -2.8eV$ and $t_1 = -0.07eV$ 25
5.4 second nearest with, $t_o = -2.8eV$ and $t_1 = -0.08eV$ 26
5.5 second nearest with, $t_o = -2.8eV$ and $t_1 = -0.09eV$ 26
5.6 second nearest with, $t_o = -2.8eV$ and $t_1 = -0.10eV$ 27
5.7 Convergence test for k point sampling of the BZ and energy cutoff. Energy is given in Rydberg units. 29
5.8 Band Structure of Graphene including all bands, σ and π. . . 30

6.1 Graphene nanoribbon band structure for 4,6 and 20 atom-width ribbons respectively. 32
6.2 Graphene nanoribbon $N_a = 4, 5, 30$ atom width respectively from top to bottom. 34

Chapter 1

Introduction

Carbon is an old but new material. It has been used for centuries going back to antiquity, but yet many new solid forms of carbon have only recently been experimentally obtained in the last few decades. Most notably, in 2004, Andre Geim and Kanstantin Novoselov [1]used a scotch tape in remarkably simple technique to extract, for the first time, a flake of carbon with a thickness of just one atom, i.e graphene, from graphite. Some other modern crystalline forms of carbon include buckyballs, carbon nanotubes (CNTs) as illustrated in Fig.1.1.

Since the discovery of Geim and Novoselov, several studies focused on the electronic structure of graphene and found that graphene has some superior properties, such as very high electron mobility[2], that makes it a promising candidate material for the electronic industry of the future [3]. The superior electronic properties of graphene are mainly attributed to its crystal structure, the 2D honeycomb lattice, and its short-range interactions. Other derivatives of graphene which share these core properties have also been subject to studies, for example 0D fullerenes, or 1D nanotubes or 2D ribbons.

Many of the highly accurate theoretical works on graphene and derivatives use first principles techniques and their findings support the possibility of using graphene based materials in industrial applications such as batteries [4] solar cells [5] catalysis [6] etc. However more reliable and realistic theoretical simulations of these applications require big scale calculations to be run, which are computationally demanding for ab initio methods.

For this reason theoretical studies also employ numerically more affordable methods such as tight binding model as used by P.R Wallace in 1947 [7]. In the tight-binding model electrons are assumed tightly bound to local attraction centers and not interacting with one another but only interacting with the lattice of ions. This allows the use of only a few atomic orbitals to represent the many body wavefunction of the material. Furthermore, in this

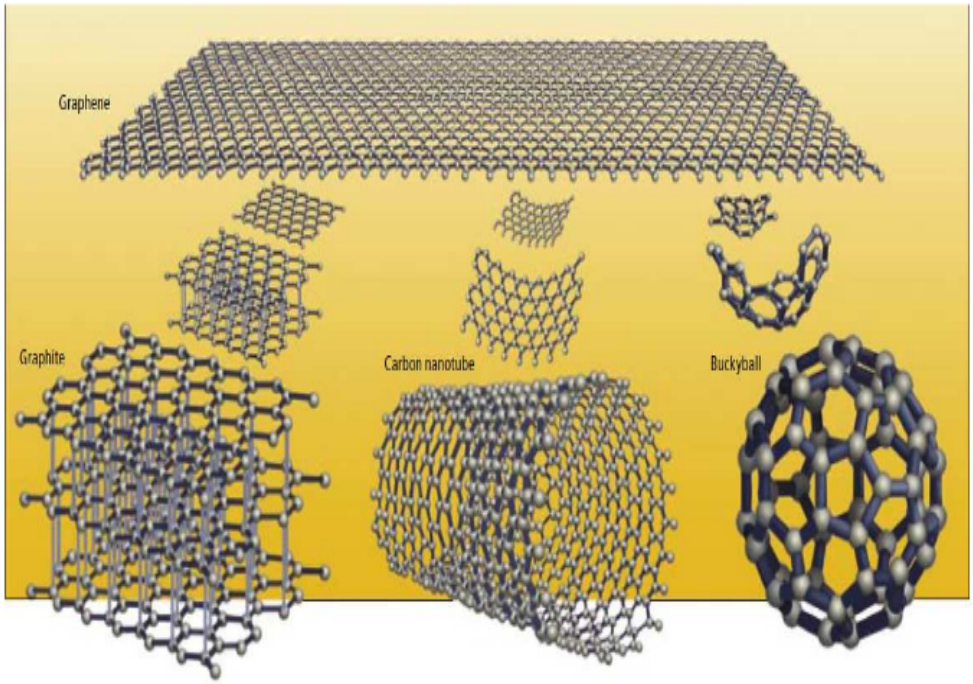

Figure 1.1: All dimensionalities of Carbon

model the integrals that describe the matrix elements of the Hamiltonian, i.e. the kinetic and potential contribution of each pair of independent electronic state of the system, can also be parametrized. The parametrization should be done such that the final tight binding description of the system coincides with truly first principles results for a wide range of systems. That way, the TB parametrization can be said to be accurate and transferable.

One successful application of TB to graphene is the work of Ref.[8] in which they demonstrate that even these simple TB approximations can qualitatively describe the important features of the band structure of graphene and CNTs with the correct parametrization.

Their research motivated us to study graphene and its derivatives such as nanoribbons with TB model using various parametrizations, and explore the relationship between atomistic structure, periodicity and electronic band structure. As in the work of [8], we then compare our results with ab initio calculations in terms of accuracy and computational efficiency so that our results can serve as a benchmark for future studies of large scale graphene-based simulations.

Chapter 2

Linear Combination of Atomic Orbitals

In this section we will discuss the origins of the Tight Binding model: atomic orbitals and their linear combinations as candidate solutions for the energy operator in a crystal. These special wavefunctions are commonly used approximations to an electron's wavefunction in the presence of an attractive Coulomb potential center such as nuclei.

2.1 H-like atom and atomic orbitals

Consider the problem of a single electron in an atomic potential (a central potential proportional to the number of protons), what is its energy spectrum and what is its wavefunction like? To answer these questions we can write the energy operator (Hamiltonian $\hat{H}$) in spherical coordinates

$$\hat{H} = -\frac{\hbar^2}{2m}\nabla^2 - \frac{Ze^2}{r} = -\frac{\hbar^2}{2m}\frac{1}{r}\partial_r^2 r + \frac{\hat{L}^2}{2mr^2} - \frac{Ze^2}{r} \tag{2.1}$$

with $Z = 1$ for a single proton (Hydrogen atom). As a solution to this equation we can suggest a separable wavefunction which is a product of two functions, that of radius and spherical angles: $\Psi(r, \theta, \phi) = R(r)Y(\theta, \phi)$. The eigenvalue equation then becomes

$$\hat{H}R(r)Y(\theta, \phi) = ER(r)Y(\theta, \phi) \tag{2.2}$$

$$\left(-\frac{\hbar^2}{2m}\frac{1}{r}\partial_r^2 r + \frac{\hat{L}^2}{2mr^2} - \frac{e^2}{r}\right) R(r)Y(\theta, \phi) = ER(r)Y(\theta, \phi) \tag{2.3}$$

But $\hat{L}^2 Y(\theta,\phi) = \hbar^2 l(l+1) Y(\theta,\phi)$, so we can write

$$\left(-\frac{\hbar^2}{2m}\frac{1}{r}\partial_r^2 r + \frac{\hbar^2 l(l+1)}{2mr^2} - \frac{e^2}{r}\right) R(r) = E R(r) \tag{2.4}$$

Let us make a substitution of $u(r) = rR(r)$, $R(r) = \frac{u(r)}{r}$ then the above equation becomes:

$$-\frac{\hbar^2}{2m}\frac{d^2u}{dr^2} + \left(\frac{\hbar^2 l(l+1)}{2mr^2} - \frac{e^2}{r}\right) u = Eu \tag{2.5}$$

Therefore we can reduce the 3D problem of the atom in a 3D central potential into a 1D problem. This equation above can be solved using asymptotic behavior and polynomial expansion. The only part one should be careful about is the r goes to zero region as we will see later.

Before we move on to solve this equation, let us make it dimensionless by defining $E = -E_o \tilde{E}$, $r = r_o \tilde{r}$, where $\tilde{E}$ and $\tilde{r}$ are dimensionless variables. This gives us the following form for the eigenvalue equation:

$$-\frac{\hbar^2}{2mr_o^2 E_o}\left(\frac{d^2}{d\tilde{r}^2} - \frac{l(l+1)}{\tilde{r}^2}\right) u - \frac{e^2}{r_o E_o}\frac{u}{\tilde{r}} = \tilde{E} u \tag{2.6}$$

We can then drop the sign over dimensionless quantities: $\tilde{E} \to E$ and $\tilde{r} \to r$. Since the equation is dimensionless then

$$\frac{\hbar^2}{2mr_o^2 E_o} = \frac{e^2}{r_o E_o} = 1 \tag{2.7}$$

Solving for the length and energy units we have $r_o = \frac{\hbar^2}{2me^2} \approx a_o/2 = 0.5 \times 0.529\mathring{A}$ (Bohr Radius) and $E_o = \frac{e^2}{r_o} = \frac{2me^4}{\hbar^2} = 4\ Ry = 4 \times 13.6eV$. Here another choice for writing a dimensionless equation would be preserving $r_0 = a_0$ and $E_o = 1\ Ry$ relations. As we can see, simple dimensionless equation already gives us some characteristic length and energy scales of the problem at hand.

2.1.1 Asymptotic analysis

Now we try to solve the dimensionless equation we wrote earlier, Eq. 2.6, at the asymptotic limits:

- **for large r**: As $r \to \infty$ the terms where r is in the denominator vanish, the derivative with respect to r term and r-independent terms

dominate, leaving a second oreder differential equation whose solution is in the form:

$$u(r) = A_1 e^{-\sqrt{E}r} + A_2 e^{\sqrt{E}r} \tag{2.8}$$

Clearly, $e^{\sqrt{E}r}$ blows up as $r \to \infty$, so we set $A_2 = 0$

$$u(r) = A_1 e^{-\sqrt{E}r} \tag{2.9}$$

- **for small r**: As $r \to 0$ the $\frac{1}{r^2}$ term dominates leaving the following differential equation to be solved:

$$\frac{d^2u}{dr^2} = \frac{l(l+1)}{r^2}u \tag{2.10}$$

whose solution is in the form of

$$u(r) = B_1 r^{l+1} + B_2 r^{-l} \tag{2.11}$$

but r^{-l} blows up near origin so we set $B_2 = 0$ leaving the solution

$$u(r) = B_1 r^{l+1}. \tag{2.12}$$

However we should keep in mind that the this argument does not apply when $l = 0$.

- We can obtain the general solution by taking the product of the above asymptotic solutions and expand the solution in the rest of the space with a polynomial function $\upsilon(r)$:

$$u(r) = \upsilon(r) r^{l+1} e^{-\sqrt{E}r} \tag{2.13}$$

where

$$\upsilon(r) = \sum_{i=0}^{\alpha} a_i r^i.$$

When we put this form for the function $u(r)$ in the complete, non-asymptotic differential equation, Eq. 2.6, we discover a recursive relation between the coefficients a_i of different order. And the fact that at the asymptotic regime the function $\upsilon(r)$ must vanish allows us to assume an end to the recursive relation (hence α must be finite), which turns out to be the relation for well-known Laguerre polynomials. Using the definition of these polynomials, the final solution to this problem can be summarized as:

$$R_{nl}(r) = \sqrt{\left(\frac{2}{a_0 n}\right)^3 \frac{(n-l-1)!}{2n((n+l)!)}} \left(e^{-\frac{r}{a_0 n}}\right) \left(\frac{2r}{a_0 n}\right)^l L_{n-l-1}^{2l+1}\left(\frac{2r}{a_0 n}\right) \tag{2.14}$$

where n, l are quantum numbers and $L(x)$ is associated Laguere polynomial, which can be written as:

$$L_n^k(x) = \frac{e^x x^{-k}}{n!} \frac{d^n}{dx^n}(e^{-x} x^{n+k}) \tag{2.15}$$

And the energy eigenvalue is

$$E_n = -\frac{e^2}{2a_0} \frac{1}{n^2} \tag{2.16}$$

where the Rydberg unit is visible as the first fraction. For ground state of hydrogen $n = 1, l = 0, m = 0$ then gives the ground state wavefunction as:

$$\Psi_{nlm} = R_{nl} Y_l^m = \Psi_{100}(r) = \frac{1}{\sqrt{\pi a_0^3}} e^{-\frac{r}{a}} \tag{2.17}$$

where Y_l^m is the spherical harmonics.

2.2 Linear Combination: H_2 dimer

Now let us move on to the problem where there are more than one attractive nuclei centers. Consider a dimer of hydrogen like atoms and two non-interacting electrons. Suppose the nuclei are placed at position R_A and R_B. The Hamiltonian for electrons is

$$\hat{H} = \hat{h_1}(r_1) + \hat{h_2}(r_2) \tag{2.18}$$

where $\hat{h_i}(r_i)$ = 1-electron hamiltonian with kinetic and potential energy operator acting on the electron i, just like in the case of Hydrogen atom but with two nuclei now. Assuming that the electrons are tightly bound to the potential centers we can think that atomic orbitals are a good basis set to describe their wavefunctions. Therefore, the eigenvector of this Hamiltonian can be written in the form of linear combination of atomic orbitals (LCAO) centered on the two atoms such as:

$$\Psi(r) = c_1\phi_1 s(r - R_A) + c_2\phi_1 s(r - R_B) = c_1\phi_1 + c_2\phi_2 \tag{2.19}$$

Using the variational principle we can find write the energy of this system as $E = \frac{\langle\Psi|\hat{H}|\Psi\rangle}{\langle\Psi|\Psi\rangle}$.

Let us now recast the eigenvalue equation for electronic energy in the matrix form:

$$\begin{pmatrix} h_{11} - ES_{11} & h_{12} - ES_{12} \\ h_{21} - ES_{21} & h_{22} - ES_{22} \end{pmatrix} \begin{pmatrix} c_1 \\ c_2 \end{pmatrix} = 0 \tag{2.20}$$

where the matrix elements are

$$\begin{aligned} h_{11} &= \langle \phi_1 | \hat{H} \phi_1 \rangle = h_{22} = h \\ h_{12} &= \langle \phi_1 | \hat{H} \phi_2 \rangle = h_{21} = -t \\ S_{11} &= \langle \phi_1 | \phi_1 \rangle = S_{22} = 1 \\ S_{12} &= \langle \phi_1 | \phi_2 \rangle = S_{21} = s \end{aligned} \tag{2.21}$$

where h is the on-site energy in the presence of other nuclei of the other atom, $-t$ ($t > 0$) is the hopping integral between basis elements centered between different atoms, and s is the overlap matrix between two two orbitals centered at different atomic position.
Turning to the eigenvalue equation, the determinant must be zero for non-trivial solutions:

$$\begin{vmatrix} h - E & -t - Es \\ -t - Es & h - E \end{vmatrix} = 0 \tag{2.22}$$

Which has two solutions

$$\begin{aligned} E_A &= \frac{h + t}{1 - s} \\ E_B &= \frac{h - t}{1 + s} \end{aligned} \tag{2.23}$$

If we assume the overlap between the two atomic orbitals to be zero for a moment, $s = 0$, we can see that the effect of the presence of a second nuclei is shifting the atomic energies symmetrically, up and down, so that the difference between the two energy levels is $2t$.

Solving for the eigenfunctions we can get the clear meaning of these new levels, which are known as Bonding and Antibonding Molecular Orbitals (MO). The result is obtained as

$$\begin{aligned} \Psi_A &= \frac{1}{\sqrt{2}} \{\phi_1 - \phi_2\} \\ \Psi_B &= \frac{1}{\sqrt{2}} \{\phi_1 + \phi_2\} \end{aligned} \tag{2.24}$$

It can be seen that the constructive addition of the two orbitals make a molecular orbital Ψ_B where the probability density is the highest between the two atoms, revealing the naming of this orbital as "Bonding orbital". It corresponds to the lower energy eigenvalue. While the subtraction eigenfunction Ψ_A, also known as "Antibonding orbital", describes zero probability density at the mid point of the atoms, and corresponds to higher eigenenergy.

We can see that the eigenvalues depends on the interatomic distance because as distance between the nuclei tends ∞, there is no possibility of electron to hop, and t would tend to zero. This indicates that the orbitals at infinite separation would be degenerate.

We can also see that the Hamiltonian commutes with angular momentum square operator $\hat{L^2}$, i.e. $[\hat{H}, \quad \hat{L^2}] = 0$ as the eigenfunctions of Hamiltonian are also the eigenfunctions of $\hat{L}^2$. Hamiltonian also commutes with the parity operator $\hat{P}$, because hamiltonian does not change by exchange of the coordinates of the 2-electrons. i.e $\hat{H}(r_1, r_2) = \hat{H}(r_2, r_1)$, bonding orbital is of even parity and the antibonding orbital is of odd parity.

2.3 Linear Combination: H trimer

We now consider an equally spaced triangular configuration of three hydrogen-like atoms i.e the hydrogen trimer. We can write 1-electron hamiltonian $\hat{h}_1$

$$\hat{h}_1 = \epsilon \sum_{i=1}^{3} |i\rangle\langle i| - t \sum_{<i,j>} |i\rangle\langle j| \tag{2.25}$$

where ϵ is the energy of 1-electron Hydrogen in the presence of two other nuclei, $|i\rangle$ is the wavefuction that represents the atomic sites of the atom localized at $i = 1, 2, 3$, and $i \neq j$. For simplicity, we can write the Hamiltonian matrix in the basis of atomic orbitals centered on each atom, as we did in the case of H-dimer, but this time assuming no overlap i.e $S_{ij} = \delta_{ij}$:

$$(H - E) \begin{pmatrix} c_1 \\ c_2 \\ c_3 \end{pmatrix} = 0 = \begin{pmatrix} \epsilon - E & -t & -t \\ -t & \epsilon - E & -t \\ -t & -t & \epsilon - E \end{pmatrix} \begin{pmatrix} c_1 \\ c_2 \\ c_3 \end{pmatrix} \tag{2.26}$$

For the non trivial solutions of the above equation we again set the determinant zero and obtain the three eigenvalues:

$$\begin{aligned} E_1 &= \epsilon - 2t \\ E_2 &= \epsilon + t \\ E_3 &= E_2 \end{aligned} \tag{2.27}$$

E_1 is the Bonding state, its eigenfunction has positive contribution from all atomic sites, it has the lowest energy possible, whereas E_2 and E_3 are

antibonding and non-bonding degenerate states. Their eigenfunctions are

$$\begin{aligned} \Psi^{\textbf{Bonding}} &\propto a\phi_1 + a\phi_2 + a\phi_3 \\ \Psi^{\textbf{Antibonding}} &\propto b\phi_1 - b'\phi_2 + b\phi_3 \\ \Psi^{\textbf{Non-bonding}} &\propto c\phi_1 - c\phi_3 \end{aligned} \tag{2.28}$$

where a,b, b' and c are normalization constants.

Chapter 3

Tight Binding Approximation

3.1 H chain and Born-von Karman boundary conditions

We know consider N-Hydrogen ring with a interatomic distance between the Hydrogen atoms. The N-ring Hydrogen atom means $\phi_{1s}^0 = \phi_{1s}^N$ where superscript denotes the number of atom where the 1s orbital is centered. The general hamiltanian, is as usual the sum of all 1-electron hamiltonian ($\hat{h}$) of hydrogen atom, since we still did not introduce electron-electron interaction:

$$\hat{H} = \sum_{i=1}^{N} h_i$$

The LCAO for $1s$ orbitals is

$$|\Psi\rangle = \sum_{\mu=1}^{N} c_\mu |\phi_{1s}^\mu\rangle$$

and the expansion of the hamiltonian in the atomic basis yields the following eigenvalue equation

$$\begin{pmatrix} H_{11} - ES_{11} & H_{12} - ES_{12} & \cdots & H_{1N} - ES_{1N} \\ H_{21} - ES_{21} & H_{22} - ES_{22} & \cdots & H_{2N} - ES_{2N} \\ \vdots & \vdots & \vdots & \vdots \\ H_{N1} - ES_{N1} & H_{N2} - ES_{N2} & \cdots & H_{NN} - ES_{NN} \end{pmatrix} \begin{pmatrix} c_1 \\ c_2 \\ \vdots \\ c_N \end{pmatrix} = 0$$

whose solution requires the solution to $N \times N$ secular equation $|\hat{H} - ES|$.

We can note that the $\hat{H}$ commutes with the translation operator $\hat{T}$ that cycles/translates the ring because, our Hamiltonian is invariant whenever we cycle any hydrogen atom to a new positions. Thus, $[\hat{H}, \hat{T}] = 0$.

To obtain the spectrum of the eigenvalue we need to solve this $N \times N$ secular equation. Using Huckel approximation i.e the ovelap follows $S_{ij} = \delta_{ij}$ and let the onsite energy be ε_o in the presence of other nuclei and the hopping integral be $(t < 0)$, the matrix can be written as:

$$\begin{pmatrix} x & 1 & 0 & 0\cdots & \cdots & 1 \\ 1 & x & 1 & 0 & \cdots & 0 \\ 0 & 1 & x & 1 & \cdots & 0 \\ \vdots & \vdots & \vdots & \vdots & \vdots & \vdots \\ 1 & 0 & 0 & \cdots & \cdots 1 & x \end{pmatrix} \begin{pmatrix} c_1 \\ c_2 \\ c_3 \\ \vdots \\ c_N \end{pmatrix} = 0 \tag{3.1}$$

where we scaled the scalars by by t and so let defined x

$$x = \frac{\varepsilon_o - E}{t}$$

We deduce the set of simultaneous equations as

$$\begin{aligned} xc_1 + c_2 + c_N &= 0 \\ xc_2 + c_1 + c_3 &= 0 \\ xc_3 + c_2 + c_4 &= 0 \\ &\vdots \\ xc_N + c_1 + c_{N-1} &= 0 \end{aligned} \tag{3.2}$$

In short we have $xc_\mu + c_{\mu+1} + c_{\mu-1} = 0$ with the boundary condition in mind.

To solve the above recursive relations let us assume the general solution as linear combination of plane waves.

$$c_\mu = Ae^{ik\mu a} + Be^{-ik\mu a}; \quad |\Psi_k\rangle = \sum_{\mu=1}^{N} (Ae^{ik\mu a} + Be^{-ik\mu a})|\phi_{1s}^{\mu}\rangle$$

Placing this in the recursive relation and with some algebra we can write

$$\begin{aligned} x(Ae^{ik\mu a} + Be^{-ik\mu a}) + Ae^{ik(\mu+1)a} + Be^{-ik(\mu+1)a} + Ae^{ik(\mu-1)a} + Be^{-ik(\mu-1)a} &= 0 \\ x(Ae^{ik\mu a} + Be^{-ik\mu a}) + Ae^{ik\mu a}(e^{ika} + e^{-ika}) + Be^{-ik\mu a}(e^{ika} + e^{-ika}) &= 0 \\ x(Ae^{ik\mu a} + Be^{-ik\mu a}) + (Ae^{ik\mu a} + Be^{-ik\mu a})(e^{ika} + e^{-ika}) &= 0 \\ (x + (e^{ika} + e^{-ika}))(Ae^{ik\mu a} + Be^{-ik\mu a}) &= 0 \\ x = -(e^{ika} + e^{-ika}) = -2\cos ka & \end{aligned} \tag{3.3}$$

which gives the eigenvalue spectrum as a shifted and scaled cosine function.

$$E = \varepsilon_o + 2t \cos ka \tag{3.4}$$

One variable we have not yet discussed is the k assumed in our suggested solution to the recursive equations. Using the PBC of the ring we can write $c_\mu = c_{\mu+N}$, which results in the following N values that k can take:

$$k = 0, \frac{2\pi}{a}\frac{1}{N}, \cdots, \frac{2\pi}{a}\frac{N-1}{N} \tag{3.5}$$

which is often shifted to equivalent and symmetric range: $(-\frac{\pi}{a}, \frac{\pi}{a})$. The N values of k all mark a specific eigenvector ($\{c_k\}$) and eigenvalue E_k.

The degeneracy depends whether N is even or odd. The lowest energy level ($k = 0$) is always non-degenerate. The highest energy is non degenerate when when N is even, else its degenerate(e.g H trimer).

3.2 Bloch Theorem

Like the H-ring we considered, real world solids are also modelled with periodic atomic potentials. Due to the periodicity of this potential, the hamiltonian operator commutes with lattice translation operator which translates the lattice by a lattice vector:

$$\hat{T_{\mathbf{R}}}\Psi = e^{i\mathbf{k}\cdot\mathbf{R}}\Psi \tag{3.6}$$

Using this, and the periodicity via Born-von Karman boundary conditions as in the case of H-ring, F. Bloch suggested that the eigenfunctions of the lattice hamiltonian are in the following form:

$$\Psi_{\mathbf{k}}(\mathbf{r}) = e^{i\mathbf{k}\cdot\mathbf{r}} u_{\mathbf{k}}(\mathbf{r}) \tag{3.7}$$

where $u_{\mathbf{k}}(\mathbf{r}+\mathbf{R}) = u_{\mathbf{k}}(\mathbf{r})$, where $\mathbf{R}$ is the lattice vector, and the wave vector $\mathbf{k}$ lies in the first brilloune zone, e.g. in 1D $(-\pi/a, +\pi/a)$. One can further introduce n quantum number, $u_{n\mathbf{k}}(\mathbf{r})$ and $\Psi_{n\mathbf{k}}(\mathbf{r})$, to account for states of different electrons, also known as bands. With this definition of $u_{\mathbf{k}}$ it is easy to see how Bloch states are eigenfunctions of the mentioned translational operator:

$$\hat{T_{\mathbf{R}}}\Psi = \Psi(\mathbf{r}+\mathbf{R}) = e^{i\mathbf{k}\cdot\mathbf{R}}\Psi(\mathbf{r}) \tag{3.8}$$

3.3 Tight binding model for graphene

In solid-state physics, the tight-binding model (TB) is an approach to the calculation of electronic band structure using an approximate set of wave functions that are superposition of isolated atom wavefunctions located at each atomic site[9]. From this point of view, TB is similar to the method of Linear combination of atomic orbitals (LCAO) used to construct molecular orbitals (MO). Like the LCAO, in the TB model, atomic wavefunctions is considered a good basis because it is assumed that the ionic potential of the atom is strong. Hence, this approximation neglects the electron-electron interactions. Due to the use of atomic orbitals as a basis, and with good parametrization however, it often yields qualitatively accurate results.

Let us now describe the basic theory behind the TB model using graphene example. To model an infinite 3D crystal or a 2D sheet, we'll always consider first a smaller system of N unit cells in periodic boundary conditions (Born-von Karman), and then consider the limiting case where N goes to infinity, as we have seen in the 1D case of H-chain earlier.

Furthermore, we will solve the Schrodinger equation of the system only for one electron from each Carbon atom, the one that belongs to p_z orbitals, because the other electrons are deeply involved in the in-layer bonds of the graphene.

The hamiltonian eigenvalue equation for a non-interacting electron in graphene has the usual kinetic and potential energy terms:

$$\left(-\frac{\hbar^2}{2m}\nabla^2 + V(r)\right)\Psi(r) = E\Psi(r) \tag{3.9}$$

where the potential is the one of the ionic lattice, after the screening of the other electrons.

In the primitive unit cell of graphene there are two atoms, we will denote as A and B. Since in the TB approximation we will use atomic orbital basis, we can denote the atomic orbitals that are centered on these atoms as ϕ_A and ϕ_B. More precisely, we can use the lattice vector to indicate the atoms these orbitals are centered on, such as $\phi_A(\mathbf{r} - \mathbf{R}_\mu) = \phi_A^\mu$ and $\phi_B(\mathbf{r} - \mathbf{R}_\mu) = \phi_B^\mu$ for the unit cell at $\mathbf{R}_\mu$.

In the case of hydrogen chain we have seen that eigenvectors were in the shape of atomic orbitals summed up with plane wave coefficients. Now we can use this information and write Bloch waves for each type of atomic

orbital we have:

$$\Psi_{A,\mathbf{k}}(\mathbf{r}) = \frac{1}{\sqrt{N}} \sum_{\mathbf{R}_\mu}^{N} e^{i\mathbf{k}\cdot\mathbf{R}_\mu} \phi_A^\mu; \qquad \Psi_{B,\mathbf{k}}(\mathbf{r}) = \frac{1}{\sqrt{N}} \sum_{\mathbf{R}_\mu}^{N} e^{i\mathbf{k}\cdot(\mathbf{R}_\mu+\delta)} \phi_B^\mu \tag{3.10}$$

where we denote the vector between A and B atoms in the same unit cell as $\delta = a/\sqrt{3}$ in the direction $\hat{x}$

Now we can rewrite our problem in the basis of these Bloch states such that the eigenvectors we are looking for are

$$\Phi_{\mathbf{k}}(\mathbf{r}) = \sum_{i=A,B} c_{i\mathbf{k}} \Psi_{i\mathbf{k}}(\mathbf{r}) \tag{3.11}$$

In this new basis the secular equation to be solved becomes

$$\begin{vmatrix} H_{AA} - E & H_{AB} \\ H_{AB}^* & H_{AA} - E \end{vmatrix} = 0 \tag{3.12}$$

$$(H_{AA} - E)^2 = |H_{AB}|^2 \tag{3.13}$$

$$E = H_{AA} \pm |H_{AB}| \tag{3.14}$$

We shall now calculate these matrix elements considering only the nearest neighbor interaction to be present.

Before continuing, let us remember the primitive unit cell of the graphene and the relationships between the neighboring atoms. Let us denote the vector between A and B atoms in the same unit cell as $\delta = a/\sqrt{3}$ in the direction $\hat{x}$, and the two lattice vectors as $\mathbf{v_1} = \sqrt{3}a/2\hat{x} + a/2\hat{y}$ and $\mathbf{v_2} = -\sqrt{3}a/2\hat{x} + a/2\hat{y}$. The difference between the positions of atom A and its nearest neighbors in other cells can be written as $-\mathbf{v_1} + \delta = -a/2\sqrt{3}\hat{x} - a/2\hat{y}$ and $+\mathbf{v_2} + \delta = -a/2\sqrt{3}\hat{x} + a/2\hat{y}$. (Different choice of primitive unit cell representations can yield different but equivalent expressions).

Usign these vector information, the diagonal term of the hamiltonian becomes

$$H_{AA} = \frac{1}{N}\sum_{\mu,\mu'} e^{-i\mathbf{k}\cdot\mathbf{R}_\mu} e^{i\mathbf{k}\cdot\mathbf{R}'_\mu} < \phi_A^\mu | H | \phi_A^{\mu'} > = \epsilon \tag{3.15}$$

$$H_{AB} = \frac{1}{N}\sum_{\mu,\mu'} e^{-i\mathbf{k}\cdot\mathbf{R}_\mu} e^{i\mathbf{k}\cdot(\mathbf{R}'_\mu+\delta)} < \phi_A^\mu | H | \phi_B^{\mu'} > \tag{3.16}$$

$$= t\left(e^{i\mathbf{k}\cdot\delta} + e^{i\mathbf{k}\cdot(-\mathbf{v_1}+\delta)} + e^{i\mathbf{k}\cdot(\mathbf{v_2}+\delta)}\right) \tag{3.17}$$

$$= t\left(e^{i\mathbf{k}\cdot\delta} + e^{i\mathbf{k}\cdot(-a/2\sqrt{3}\hat{x}-a/2\hat{y})} + e^{i\mathbf{k}\cdot(-a/2\sqrt{3}\hat{x}+a/2\hat{y})}\right) \tag{3.18}$$

$$= t\left(e^{i\mathbf{k}\cdot\delta} + e^{-ik_x a/2\sqrt{3}} e^{-ik_y a/2} + e^{-ik_x a/2\sqrt{3}} e^{ik_y a/2}\right) \tag{3.19}$$

$$= t\left(e^{i\mathbf{k}\cdot\delta} + e^{-ik_x a/2\sqrt{3}} 2cos(k_y a/2)\right) \tag{3.20}$$

$$= t\left(e^{ik_x a/\sqrt{3}} + e^{-ik_x a/2\sqrt{3}} 2cos(k_y a/2)\right) \tag{3.21}$$

where we have reused the previously defined on-site and hopping terms $\epsilon = \langle\phi_A^\mu|H|\phi_A^\mu\rangle$ and $t = \langle\phi_A^\mu|H|\phi_B^\mu\rangle$. This allows us to write the eigenvalues as

$$E_{\mathbf{k}} = E_{k_x,k_y} = \epsilon \pm t\left|e^{ik_x a/\sqrt{3}} + e^{-ik_x a/2\sqrt{3}} 2cos(k_y a/2)\right| \tag{3.22}$$

with further algebra it can be cast as:

$$E(\mathbf{k}) = \epsilon + t\left[1 + 4\cos\left(\frac{\sqrt{3}k_x a}{2}\right)\cos\left(\frac{k_y a}{2}\right) + 4\cos^2\left(\frac{k_y a}{2}\right)\right]^{\frac{1}{2}} \tag{3.23}$$

where high energy band corresponds to eigenvectors formed by anti-bonding π^* orbitals and low energy band indicates valence band formed by bonding π orbitals.

Chapter 4

Density functional theory

Density functional theory (DFT) is a quantum mechanical modelling formalism used to investigate the electronic structure of many-body systems at the ground state[10]. The name density functional theory comes from the use of functionals of the electron density. Density functional theory has its roots from the Thomas–Fermi model for the electronic structure of materials, DFT was then first put on a firm theoretical footing by Walter Kohn and Pierre Hohenberg in the framework of the two Hohenberg–Kohn theorems (HK) [11]

4.1 Formalism

In 1927, Born-Oppenhiemer approximation(adiabatic approximation) was introduced to decouple the motion between the nuclei and electrons. Since nuclei is much heavier than electron, the approximation is that that nuclei do not move as we solve for the motion of electrons, i.e. the time scale of ionic dynamics is much longer than that of electrons[12]. This becomes helpful in neglecting the ionic motion in many-body calculations while solving for electronic steady states. As a result, the total wavefunction is considered as $\Psi_{TOTAL} = \Psi_{ELCTRON} \times \Psi_{NUCLEAR}$ [13]

Thus we can write the Hamiltonian of many-body system in the adiabatic approximation:

$$H = -\sum_{i}^{n} \frac{\hbar^2}{2m} \nabla^2_{\mathbf{r}_i} + \sum_{i \neq j} \frac{e^2}{|\mathbf{r}_i - \mathbf{r}_j|} - \sum_{i,I} \frac{Z_I e^2}{|\mathbf{r}_i - \mathbf{R}_I|} \tag{4.1}$$

Where $\mathbf{r}$ and $\mathbf{R}$ are the electron and the nuclei positions and n is the number of electrons. The last term in the above equation is the external potential energy $\hat{V}$ sometimes written as V_{ext} which clearly depends on the nuclei positions.The first and the second term are the electron kinetic energy $\hat{T}$

and interacting potential energy $\hat{U}$. The expectation value of the above hamiltonian over the many body wavefunction of electrons is:

$$E = \iiint \dots \int \Psi^* \left(\sum_i^N \frac{\hbar^2}{2m} \nabla^2_{\mathbf{r}_i} + \sum_{i \neq j} \frac{e^2}{|\mathbf{r}_i - \mathbf{r}_j|} - \sum_{i,I} \frac{Z_I e^2}{|\mathbf{r}_i - \mathbf{R}_I|} \right) \Psi d\mathbf{r}_1 d\mathbf{r}_2 \dots d\mathbf{r}_n \tag{4.2}$$

Clearly, above equations is hard to handle because the many body wavefunction is written in a $3n$ dimensional space. DFT allows us to work with the electronic density rather than the many body wavefunction. The density is only a function of 3 degrees of freedom:

$$n_0(\mathbf{r}) = \iiint \dots \int |\Psi_0(\mathbf{r}, \mathbf{r}_2, \mathbf{r}_3, \dots, \mathbf{r}_n)|^2 d\mathbf{r}_2 d\mathbf{r}_3 \dots d\mathbf{r}_n \tag{4.3}$$

HK theorem tells us that the ground state energy can be written as a functional of ground state density as[12] :

$$E[n_0] = T[n_0] + U[n_0] + \int V(\mathbf{r}) n_0(\mathbf{r}) d\mathbf{r} \tag{4.4}$$

The functional $F[n_0] = T[n_0] + U[n_0]$ is called universal functional because only the $V[n_0]$ term depends on the external conditions of the ions while the others must be universal for all ground state electron densities independent of the ions and their positions.

Kohn and Sham showed if all that matters is the ground state density, one can map this interacting many body system to a non-interacting one, as long as one has the same electronic density[12] and the electron electron interaction can be remapped as part of the external potential.

$$\left[-\frac{\hbar^2}{2m} \nabla^2 + V_s(\mathbf{r}) \right] \phi_i(\mathbf{r}) = \varepsilon_i \phi_i(\mathbf{r}) \tag{4.5}$$

Where V_s is the external effective potential in which the particles are moving and $\phi_i(\mathbf{r})$ are called the Kohn-Sham orbitals. The effective single-particle potential can be written in more detail

$$V_s(\mathbf{r}) = V(\mathbf{r}) + \int \frac{e^2 n(\mathbf{r}')}{|\mathbf{r} - \mathbf{r}'|} d\mathbf{r}' + V_{XC}[n(\mathbf{r})] \tag{4.6}$$

where we imagined to split the effective potential into an ionic term, a simple mean-field term and a more complex term that we do not yet described. The second term is the so-called Hartree term, it describes the electron-electron

Coulomb repulsion via mean-field approximation, the simplest approximation we can make to many body e-e interaction, while in the last term we gather all the differences between this non-interacting picture and the interacting one we do not know. This term, V_{XC}, is called the exchange-correlation potential[12]. In Kohn-Sham picture we can solve for the single electron wavefunctions using the potential, and obtain the density and then obtain the potential as a functional of the density. Because of this interdependence of potential and density, the problem of solving the Kohn–Sham equation is done in a self-consistent (i.e., iterative) way[14]. Usually one starts with an initial guess for $n(\mathbf{r})$, then calculates the corresponding V_s and solves the Kohn–Sham equations for the ϕ_i. From these one calculates a new density and starts again. This procedure is then repeated until convergence is reached. From above equation we can determine the ecxhange energy functional by taking the variational derivative w.r.t to the density evaluated at the ground state density.i,e

$$E_{xc}[n(\mathbf{r})] = \frac{\delta V_{xc}}{\delta n(\mathbf{r})} \tag{4.7}$$

But still we did not describe what the Exchange energy functional is like. Indeed, apart from a few toy systems, the exact exhange and correlation energy functional is not known, and this is an active research field. The simplest functional approximation used nowadays is the Local Density approximation (LDA) derived from Homogeneous electron gas model (HEG) where LDA functional depends only on the density at the coordinate where the functional is evaluated. For a spin-unpolarized system, a local-density approximation for the exchange-correlation energy is written as[12]:

$$E_{xc}^{LDA}[n(\mathbf{r})] = \int n(\mathbf{r})\varepsilon_{xc}^{homo}(n(\mathbf{r}))d\mathbf{r} \tag{4.8}$$

where ε_{xc}^{homo} is the exchange-correlation energy per particle of a homogeneous electron gas of charge density n. Commonly the exchange correlation energy is written as sum of exchange and correlation parts and different approximations are done on each in order to approximate the exchange correlation functional:

$$E_{xc} = E_x + E_c \tag{4.9}$$

Other functional form that is commonly used in DFT calculations is Generalized Gradient Approximation (GGA) where the functional depends on both density and its gradients due to non-homogeneity of the density, in order to resolve the shortcomings of LDA. Among the widely use GGA functional is PBE functional by Perdew, Burke, and Ernzerhof[15] which we used in thesis.

4.2 Pseudopotentials

Many solid state codes implement DFT utilize planewave basis in the solution of Kohn-Sham equations. Indeed we have previously seen how planewave coefficients are suitable for problems with periodic boundary conditions. One drawback of using planewaves as a basis is the fact that the more localized an electronic state is in real space, the more planewaves are needed in its expansion. Therefore, if one wants to describe a 3s orbital and a 1s orbital of an atom with the same accuracy; one would need a lot of plane waves due to the more localized one. Primarily for this reason, the computational DFT community has long made use of "pseudopotentials", which is a practice that suggests a different treatment for very localized and rather delocalized states of the atom.

In practice pseudopotential theory suggests that the electronic states of an atom can be divided into core and valence electronic states considering the energy of the orbitals and their spatial expansion. For example Si, total electron number is 14, the electron shell structure orbit is $1s^2 2s^2 2p^6 3s^2 3p^2$ with $1s^2 2s^2 2p^6$ as core and $3s^2 3p^2$ as valence electronic states. In many environments relevant for chemistry and solid state physics, the core electronic states are mostly occupied and does not vary from one environment to another, while the chemical properties strongly depend on the wavefunction of the valance electrons. Therefore a first approximation we can do is to treat the core as frozen in atomic configuration and treated Si atom in other environments as having only 4 electrons and an ionic core. This way we group the 10 core electrons and the nuclei into an effective potential, which is the so called pseudo-potential that the valance electrons experience. In order to produce accurate results with this model, one criterion that is kept is that the real potential of the atom and the model potential match exactly beyond a radius that is often called the cut-off radius.

There are various techniques to generate pseudo-potentials depending on choice of atomic core cut-off radius, and some other important concepts that we summarize as below:

- Norm-conservation: Using the pseudopotential in the atomic environment we can solve the pseudo wavefunction of the valance states and compare them with the real valance wavefunctions. If the norm of the pseudo valance wavefunction up to the cut-off radius r_c is the same as the non-approximated, real valance wavefunction we call this a norm-conserving pseudopotential. This condition often results in hard pseudopotentials

- Softness-hardness: The pseudopotentials are often used in solid state

environments where the hamiltonian and wavefunctions are expanded in plane wave basis set. Therefore it is very useful to make pseudopotentials such that the plane wave expansion of the solutions, ie the valance pseudo wavefunctions can be expressed in small number of planewaves. This quality, the number of planewaves required, is often referred as softness of a pseudopotential. It is useful in comparing the computational cost associated with the use of different pseudopotentials. Softness is a desired quality. For example, Ultrasoft pseudopotentials developed by Vanderbilt avoid the norm conservation constraint for accommodating softer potentials, and are therefore one of the most popular choices in the community.

- Transferability: The pseudo-potential generated for an atom should be readily usable in several different solid state and molecular environments.

Chapter 5

Graphene

Graphene is a honeycomb lattice structure which can be described in terms of 2-triangular sub-lattices A and B [16] as shown in the figure below. Graphene contains 2 atoms per unit cell with primitive unit vectors $\mathbf{a_1}$ and $\mathbf{a_2}$ describing the triangular lattices.

$$\mathbf{a_1} = a/2(1, \sqrt{3}) \tag{5.1}$$

$$\mathbf{a_2} = a/2(-1, \sqrt{3}) \tag{5.2}$$

Where $a = \sqrt{3}d_{cc}$ [16]is lattice constant and d_{cc} is a carbon-carbon bond length. The unit vectors in reciprocal lattice $\mathbf{b_1}$ and $\mathbf{b_2}$ are defined as

$$\mathbf{b_1} = 2\pi \frac{(\mathbf{a_2} \times \hat{\mathbf{z}})}{\mathbf{a_1} \cdot (\mathbf{a_2} \times \hat{\mathbf{z}})} \tag{5.3}$$

$$\mathbf{b_2} = 2\pi \frac{(\hat{\mathbf{z}} \times \mathbf{a_1})}{\mathbf{a_1} \cdot (\mathbf{a_2} \times \hat{\mathbf{z}})} \tag{5.4}$$

$$\mathbf{b_1} = \frac{2\pi}{\sqrt{3}a}(\sqrt{3}, 1) \tag{5.5}$$

$$\mathbf{b_2} = \frac{2\pi}{\sqrt{3}a}(-\sqrt{3}, 1) \tag{5.6}$$

The first Brillouin zone is hexagonal which have 6 symmetry axis $\mathbf{K}$ and $\mathbf{K}$‘ which can be differentiated from one another by $\pi/6$ rotations and invariant by $\pi/3$ rotations[17]. Using the symmetry of the crystal, the first Brillouin zone (BZ) can be reduced to the smaller irreducible Brillouin zone (IBZ) as shown as half of an equilateral triangle with vertices at $\mathbf{\Gamma}$, $\mathbf{M}$ and $\mathbf{K}$. The IBZ is therefore the unique region of the BZ. The high symmetry

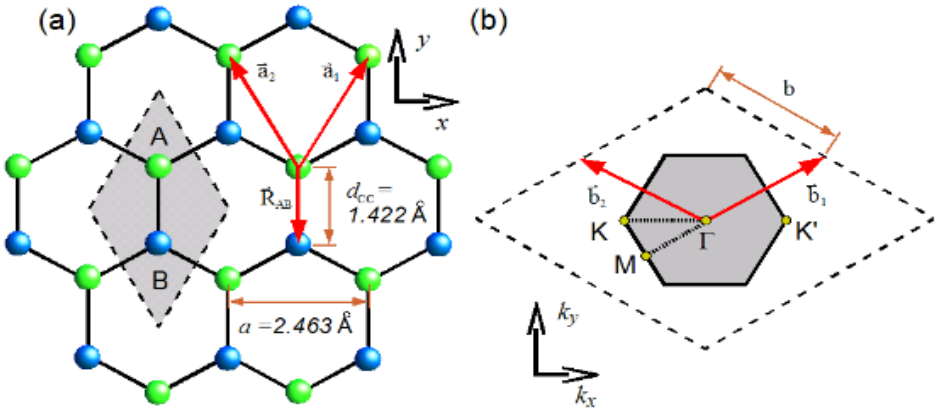

Figure 5.1: (a): Graphene with its sub-lattices. (b): The first brilloune zone and the IBZ

paths along the IBZ, such as $\mathbf{\Gamma} - \mathbf{K}$, are often used to demonstrate electronic band structure of a material.

Each Carbon atom in the graphene has four valence electrons. Three of these electrons are involved in the intra layer bonds of the graphene: 2s and 2px and 2py orbitals hybridize in what is known as the sp2 hybridization. The 2pz orbital points out of plane. The pz orbitals overlap in side-wise manner with one another, much more weakly than the face-to-face overlap of intra-layer sp2 hybrid bonds. Therefore pz orbitals remain similar to their atomic shape, and are singly occupied. This allows us to model graphene with one orbital per atom, like H-chain. As in the case of H-chain, the eigenvectors of this pz-subsystem are in the shape of atomic orbitals with bonding or antibonding combinations.

5.1 Tight Binding Results

In this section we solve the tight binding equations that were described previously for the case of graphene. As a result we report the band structure in the K,Γ,M,K pathway in the BZ. We also plot the density of states which tell us the number of states per unit energy that electrons are allowed to occupy:

$$D(E) = \sum_{n,\mathbf{k}\in BZ} \delta(E - E_n(\mathbf{k})) \tag{5.7}$$

where n is the band index. Density of states is an important property to examine for a material, in particular to understand electron transport in a material. A high density of states around the fermi energy often indicates a good conductor.

The numerical solution of tight binding equations are done using the PythTB code with parameters obtained by Kundu[18] that re-fit the parameter sets obtained by Reich [8] by increasing the neighbour distance. The basic parameters to fit were the on-site, hopping energy and overlap energy for both nearest and second nearest sites.

TB with first nearest neighbour interaction

In this model we have considered only nearest neighbor interaction, therefore there are three parameters were needed to describe the Hamiltonian: i) onsite interaction ϵ_0, ii) A-B hopping for nearest neighbors t_0 iii) overlap integral between orbitals centered on adjacent A and B atoms s_{AB}. We have set ϵ_0 to zero, and used $t_0 = -2.74eV$ and $s_{AB} = 0.065eV$ as in the reference [18]. And then we have compared this result to the ones of two other parameter choice: $t_0 = -2.8eV$ and $t_0 = -3.0eV$. As we expect from the TB theory, this increase in the hopping parameter does not qualitatively change the band structure but only quantitatively. When the results are compared to the parameter-free ab initio calculation presented in Fig.5.8, we can see that the qualitative description of the pz bands using TB model only with nearest hopping agrees with the ab initio results: The well-known Dirac point appears at K, where conduction and valance bands join at single point at Fermi energy. This is the feature that is responsible for the conductivity of Graphene and is also responsible for the linear regime in the DoS - even though it cannot be fully appreciated in our DoS calculations due to lack of precision. Furthermore, one can also observe the flat band at M saddle point in the TB model, qualitatively in agreement with the ab initio Graphene band structure.

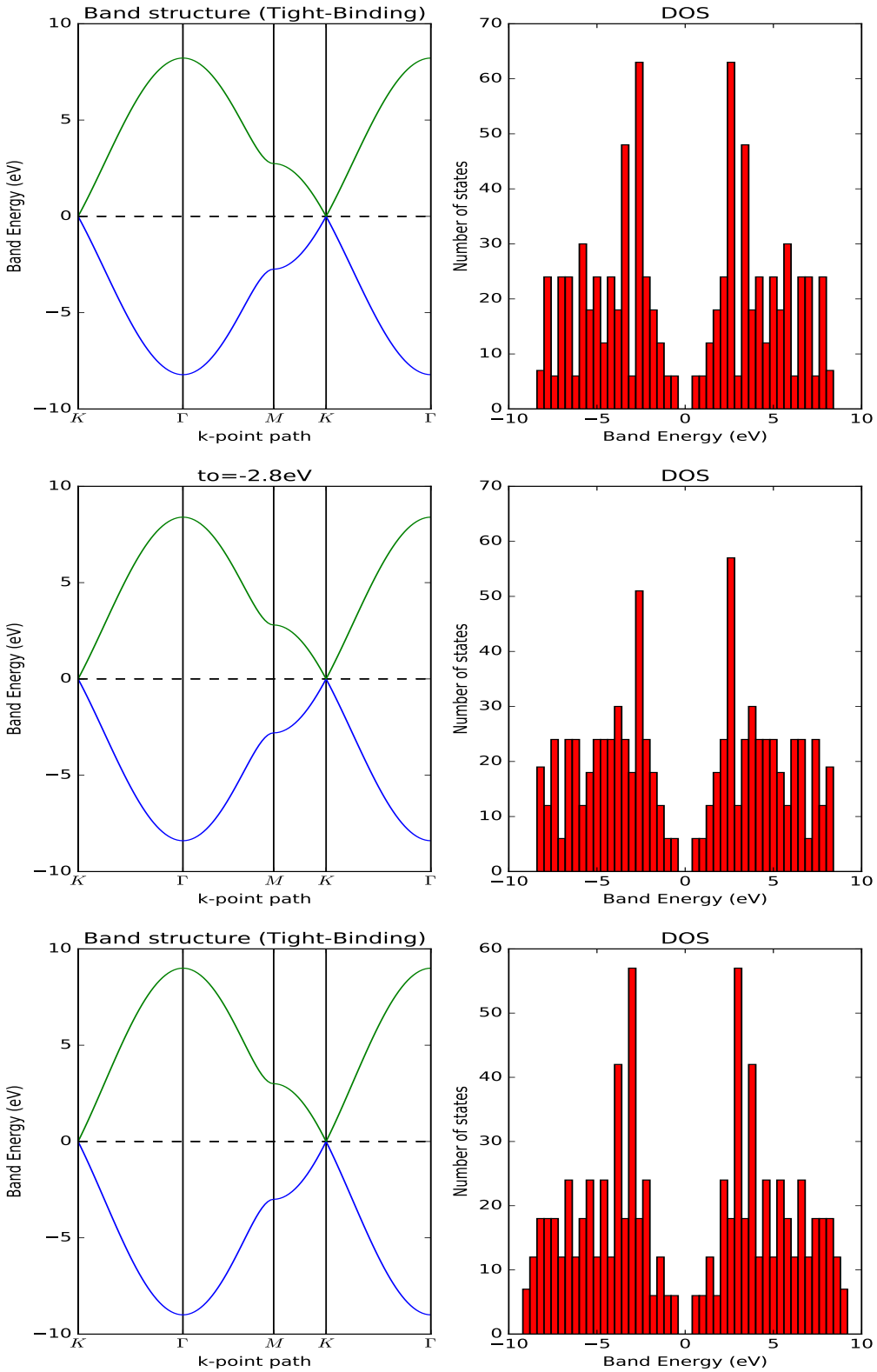

Figure 5.2: PythTB calculations of Graphene, t_0 values used are 2.74eV(top), 2.80eV(mid), 3.00eV(bottom panel).

Second nearest neighbour

Now we take another set of parameters from literature, namely Ref.[[18]] and solve a TB model with second nearest site hopping is included. In this model the parameters we use, in addition to t_o and s_{AB} from first nearest neighbour model, are $\varepsilon_o = -0.21eV, s_{AA'} = 0.002eV, t_1 = 0.07eV$. In Figures **??** and 5.6 we present slight variations on the second nearest neighbor hopping, by changing it in the range of 0.007-0.010 eV. You can see in the results that addition of second nearest neighbor interaction changes slightly the band width. It can also be seen in DoS that with this model, the DoS is no more symmetric between valance and conduction bands, therefore electron and hole conductance would not be symmetric with this model.

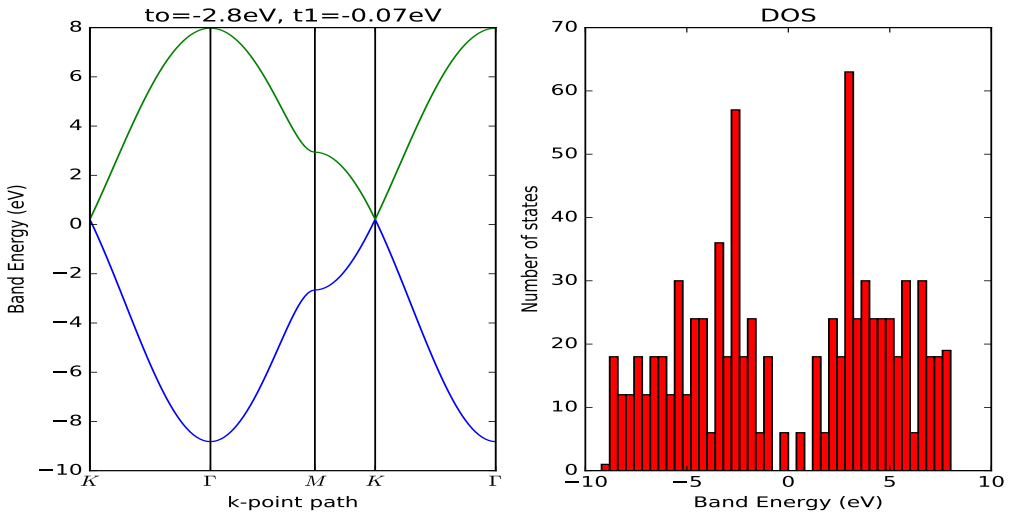

Figure 5.3: second nearest with, $t_o = -2.8eV$ and $t_1 = -0.07eV$

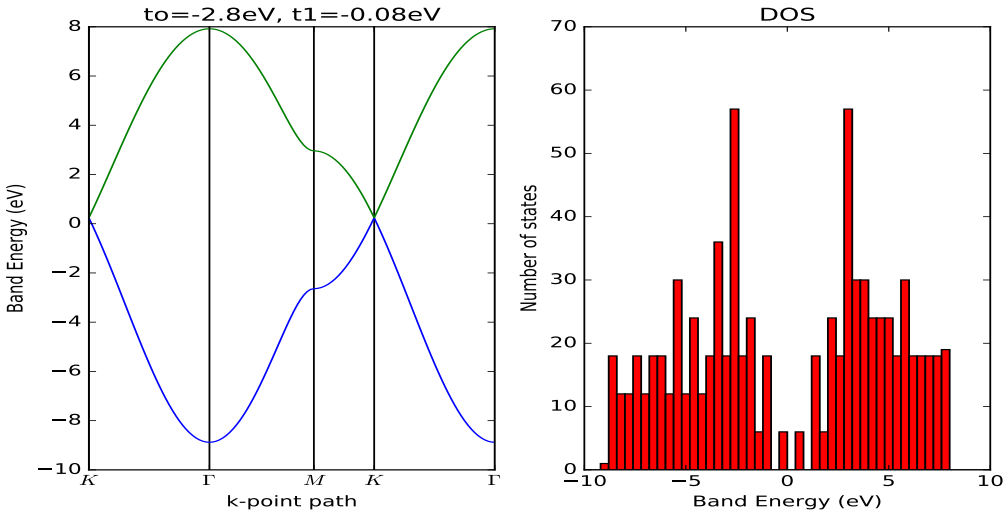

Figure 5.4: second nearest with, $t_o = -2.8eV$ and $t_1 = -0.08eV$

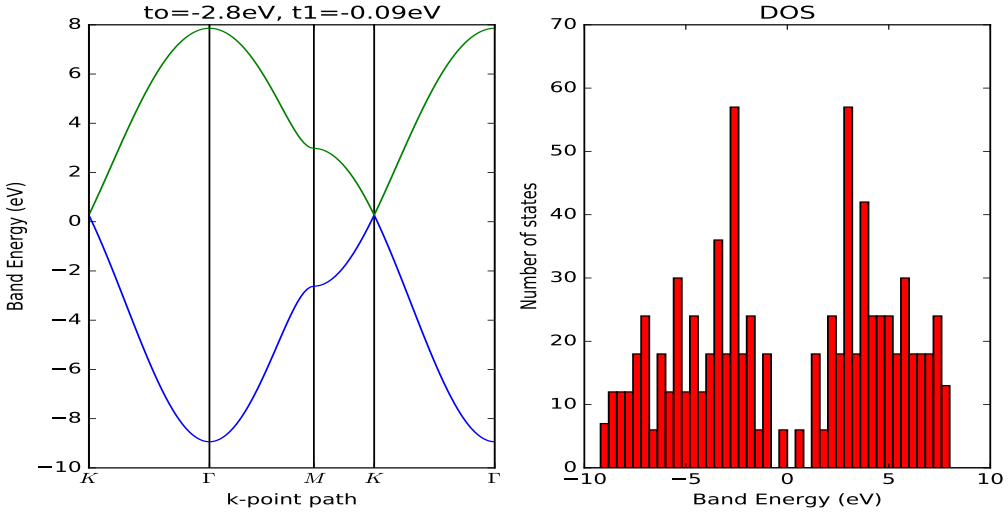

Figure 5.5: second nearest with, $t_o = -2.8eV$ and $t_1 = -0.09eV$

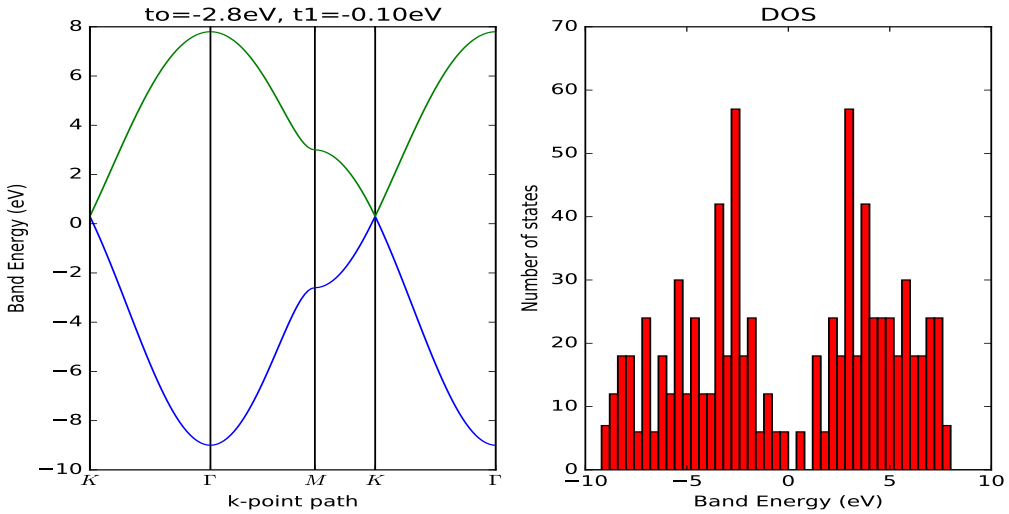

Figure 5.6: second nearest with, $t_o = -2.8eV$ and $t_1 = -0.10eV$

5.1.1 Ab-initio result

Ab initio calculations are performed in the framework of Density Functional Theory using Quantum Espresso (QE) open source suite of codes [19]. The calculation was done using Perdew-Burke-Ernzerhof (PBE) Functional and at the experimentally determined cell parameter $a = 2.46\mathring{A}$ [20]. An ultrasoft pseupotential with kinetic energy cutoff of 55Ryd, density cutoff of 300Ryd and k-point mesh of $8 \times 8 \times 1$ was chosen. Using these input parameters, total energy was converged within a threshold 1 mRyd per atom as shown in Fig5.7.

In Figure 5.8 we report the full band structure of graphene, including both σ and π energy bands. The degeneracy at the **K** point, i.e the Dirac point, is visible. The bands that meet at **K** are partially filled, identifying correctly that graphene is gapless and would conduct electricity. Furthermore, in the vicinity of **K** point the dispersion relation is linear.

The linear dispersion of energy as a function of momentum is the property of a massless particle that solves Dirac's relativistic equation. Therefore we can say that the quasiparticles in graphene around the crystal momentum **K** behave like massless relativistic particles. We can also see that the bonding and antibonding π bands are far from symmetric in the case of ab initio calculations, unlike the symmetric nearest neighbor without hopping approximation in TB, and more like TB results with next nearest hopping and overlap.

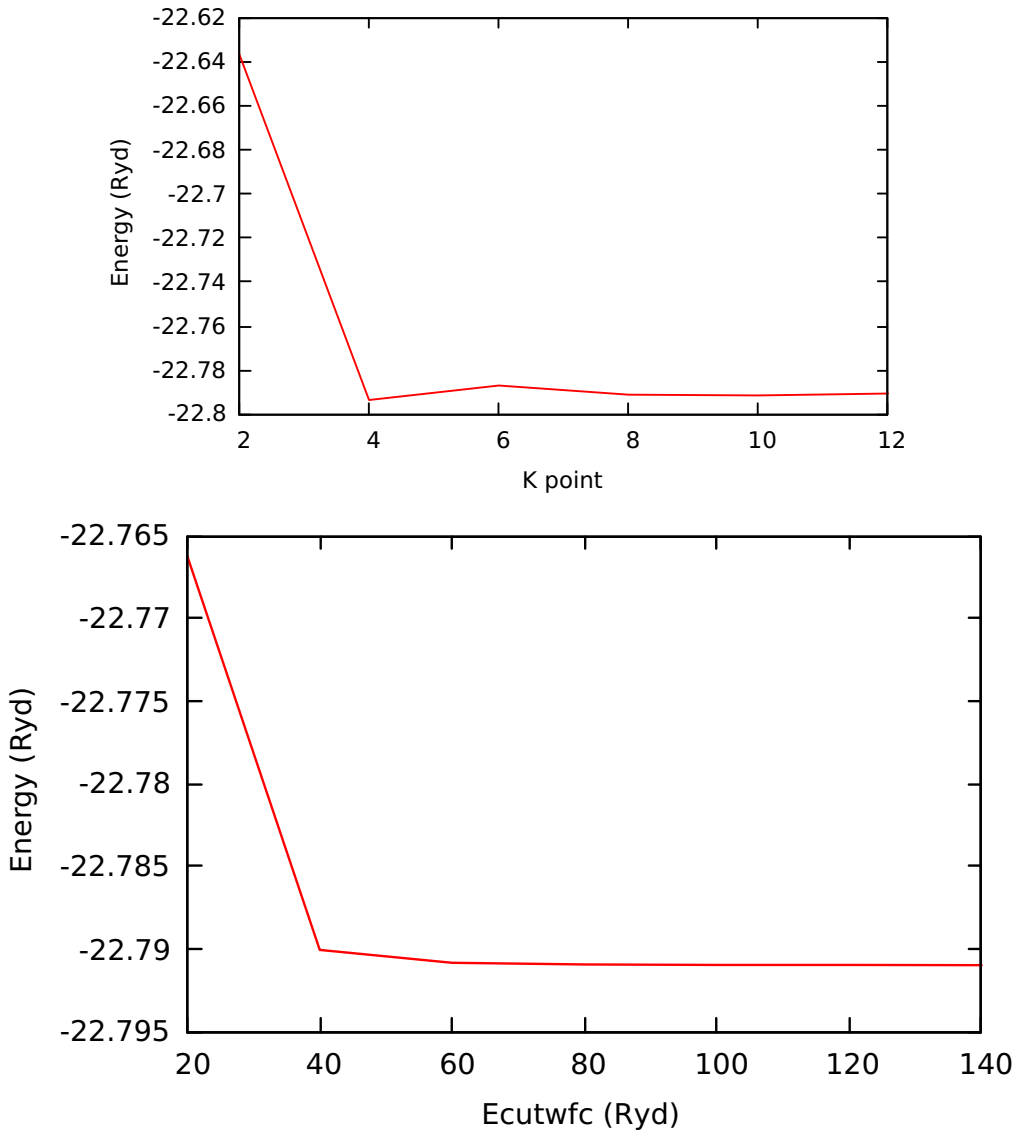

Figure 5.7: Convergence test for k point sampling of the BZ and energy cutoff. Energy is given in Rydberg units.

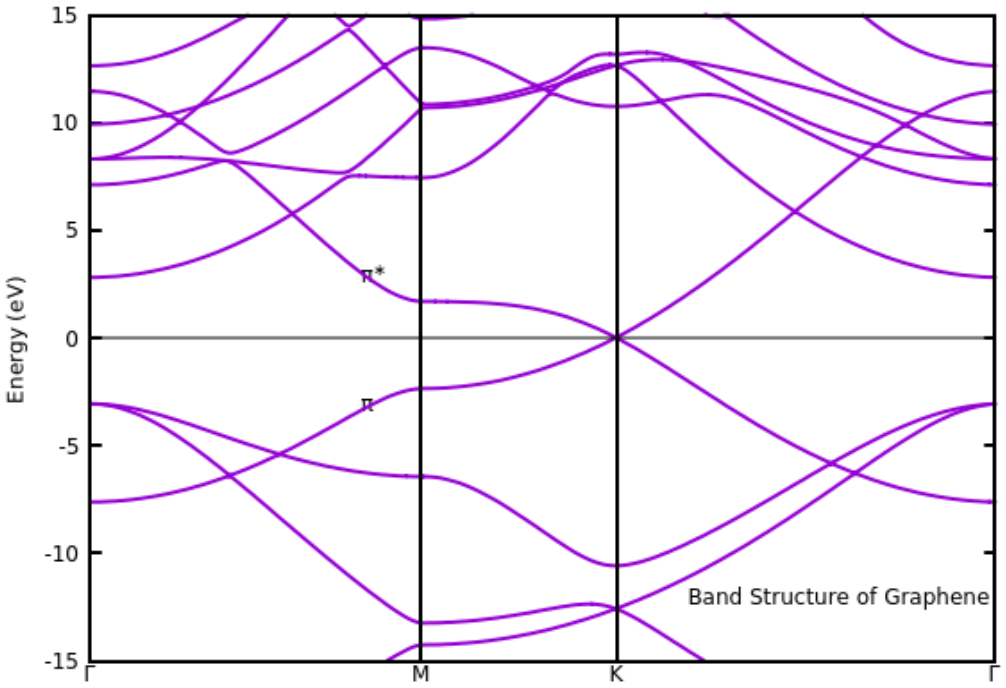

Figure 5.8: Band Structure of Graphene including all bands, σ and π.

Chapter 6

Nanoribbons

Graphene nanoribbons are strips of graphene with width less than 50 nm. Graphene ribbons were studied theoretically to examine the edge states long before the experimental extraction of these materials [21]. Nanoribbons show distinct electronic properties when compared to two-dimensional graphene, and they are named either armchair or zigzag based on the termination.

6.1 Results for Zigzag Ribbon (zGNR)

Using the nearest-neighbor tight-binding Hamiltonian with single p_z orbital per carbon atom, the band structure of three zGNR with widths $N_z = 4, 6, 20$ are shown in figure 6.1. As it can be seen this structure always have a band that is in the gap, that crosses the Fermi level, therefore this material is always a conductor independent of the ribbon width.

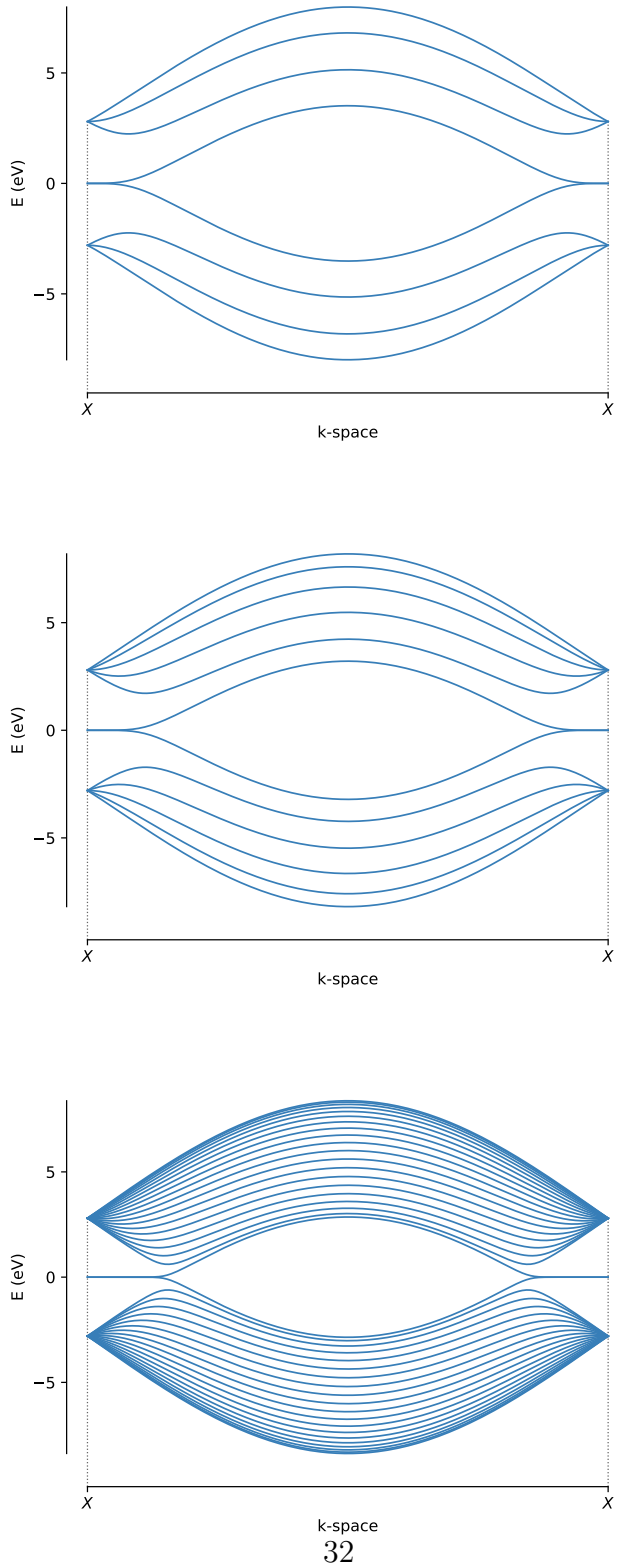

Figure 6.1: Graphene nanoribbon band structure for 4,6 and 20 atom-width ribbons respectively.

6.2 Results for Armchair Ribbon (aGNR)

With the same set of TB parameters with nearest neighbor hopping as in the case of graphene and zigzag ribbon, here we report our results for the arm-chair ribbon with width $N_a = 4, 5, 30$ atoms (See Fig.6.2). We see that the band structure changes characteristics depending on the width, becomes gapped or gapless. The gapless state resembles very closely to the state in the gap that is observed for the zigzag ribbon, which closely resembles the original π band of graphene at Dirac point.

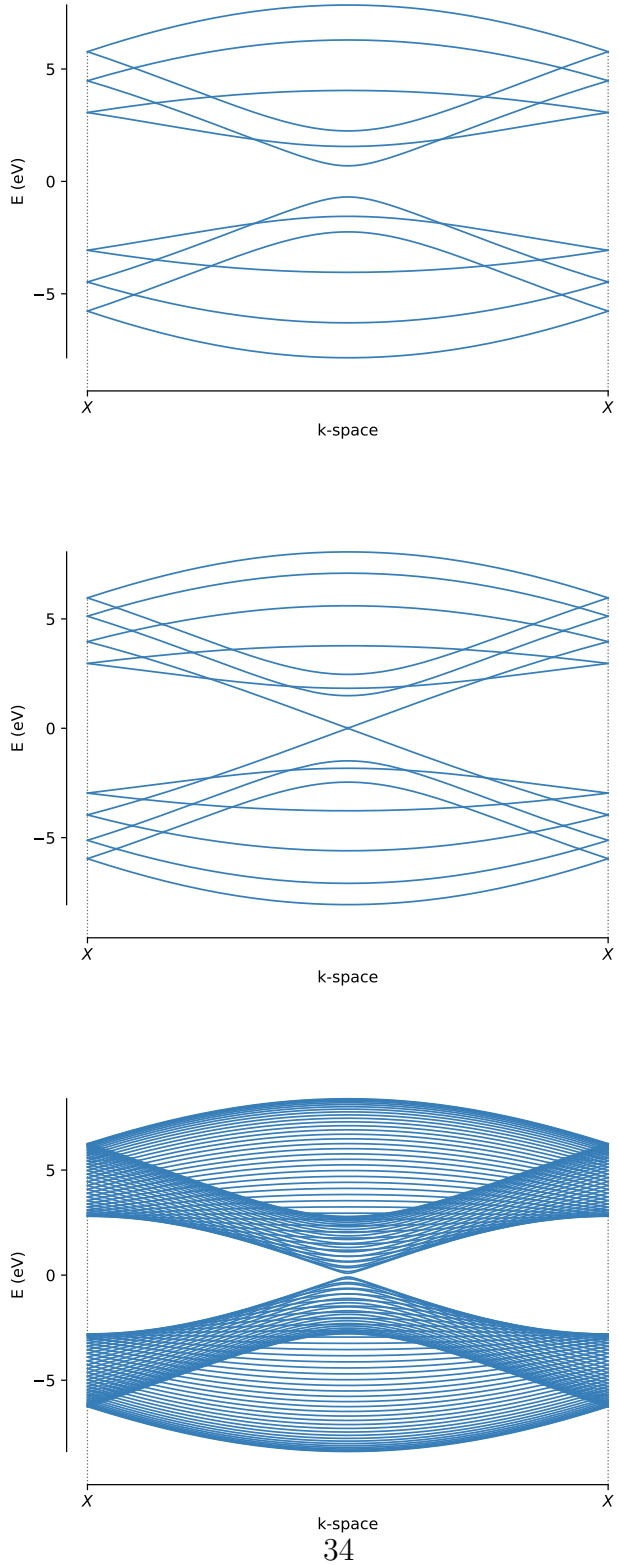

Figure 6.2: Graphene nanoribbon $N_a = 4, 5, 30$ atom width respectively from top to bottom.

Chapter 7

Conclusion and Outlook

We have validated that the results of the tight binding method for 2D graphene with the state of the art parameters from literature agree well with the DFT calculation qualitatively, especially around the Dirac point [8, 18]. While the first nearest neighbor hopping alone appears to be insufficient to account for the asymmetry of conduction and valance π bands, adding further interaction parameters and overlap accordingly, remedies this feature for tight binding model.

We also studied the band structure of nanoribbons using, for simplicity, only nearest neighbor hopping approximation in tight binding. We see from the band structure calculation that zig-zag nanoribbon is metallic irrespective of the width of the ribbon while the same conclusion can not be said about arm-chair nanoribbon because it can be gapless depending on the width.

The relationship between graphene and ribbon band structures can be understood considering that the primitive unit cell of ribbons are repeating and rotated ones of graphene, therefore the brilluoin zone of nanoribbons can be approximated as folded ones of graphene. This relationship reveals the similarities of graphene and nanoribbon band structures we calculated and can be fully accounted for with the tight binding calculations. In future studies we plan to investigate this relationship further and extend the mapping from graphene Brillouin zone to the Brillouin zone of other graphene derivatives such as nanotubes.

Bibliography

[1] K. S. Novoselov et.al. Electric field effect in atomically thin carbon films. *Nature Physics*, 6, Sep 2004.

[2] S. Das Sarma, Shaffique Adam, E. H. Hwang, and Enrico Rossi. Electronic transport in two-dimensional graphene. *Rev. Mod. Phys.*, 83:407–470, May 2011.

[3] Caiyun Wang, Dan Li, Chee O. Too, and Gordon G. Wallace. Electrochemical properties of graphene paper electrodes used in lithium batteries. *Chemistry of Materials*, 21(13):2604–2606, 2009.

[4] Seung-Min Paek, EunJoo Yoo, and Itaru Honma. Enhanced cyclic performance and lithium storage capacity of sno2/graphene nanoporous electrodes with three-dimensionally delaminated flexible structure. *Nano Letters*, 9(1):72–75, 2009. PMID: 19090687.

[5] Zongyou Yin, Jixin Zhu, Qiyuan He, Xiehong Cao, Chaoliang Tan, Hongyu Chen, Qingyu Yan, and Hua Zhang. Graphene-based materials for solar cell applications. *Advanced Energy Materials*, 4(1):1300574–n/a, 2014. 1300574.

[6] Yanguang Li, Hailiang Wang, Liming Xie, Yongye Liang, Guosong Hong, and Hongjie Dai. Mos2 nanoparticles grown on graphene: An advanced catalyst for the hydrogen evolution reaction. *Journal of the American Chemical Society*, 133(19):7296–7299, 2011. PMID: 21510646.

[7] P. R. Wallace. The band theory of graphite. *Phys. Rev.*, 71:622–634, May 1947.

[8] S. Reich, J. Maultzsch, C. Thomsen, and P. Ordejón. Tight-binding description of graphene. *Phys. Rev. B*, 66:035412, Jul 2002.

[9] Wikipedia. The free encyclopedia, 2018.

[10] Wikipedia. The free encyclopedia, 2018. [Online; accessed 03-March-2017].

[11] P. Hohenberg and W. Kohn. Inhomogeneous electron gas. *Phys. Rev.*, 136:B864–B871, Nov 1964.

[12] A/P Wang Jian-Sheng. *Lecture note of Computational Condensed Matter Physics*, chapter 2.1. Typeset by Yang Shiyang, June 1999.

[13] Wikipedia. The free encyclopedia, 2018. [Online; accessed 03-March-2017].

[14] W. Kohn and L. J. Sham. Self-consistent equations including exchange and correlation effects. *Phys. Rev.*, 140:A1133–A1138, Nov 1965.

[15] John P. Perdew, Kieron Burke, and Matthias Ernzerhof. Generalized gradient approximation made simple. *Phys. Rev. Lett.*, 77:3865–3868, Oct 1996.

[16] A. H. Castro Neto, F. Guinea, N. M. R. Peres, K. S. Novoselov, and A. K. Geim. The electronic properties of graphene. *Rev. Mod. Phys.*, 81:109–162, Jan 2009.

[17] Zhiping Xu. *GRAPHENE, properties,synthesis and Applications*, chapter 3.2. Nova Science Publishers, Inc., 2011.

[18] Rupali Kundu. Tight-binding parameters for graphene. *Modern Physics Letters B*, 25(03):163–173, 2011.

[19] P Giannozzi, O Andreussi, T Brumme, O Bunau, M Buongiorno Nardelli, M Calandra, R Car, C Cavazzoni, D Ceresoli, M Cococcioni, N Colonna, I Carnimeo, A Dal Corso, S de Gironcoli, P Delugas, R A DiStasio Jr, A Ferretti, A Floris, G Fratesi, G Fugallo, R Gebauer, U Gerstmann, F Giustino, T Gorni, J Jia, M Kawamura, H-Y Ko, A Kokalj, E Küçükbenli, M Lazzeri, M Marsili, N Marzari, F Mauri, N L Nguyen, H-V Nguyen, A Otero de-la Roza, L Paulatto, S Poncé, D Rocca, R Sabatini, B Santra, M Schlipf, A P Seitsonen, A Smogunov, I Timrov, T Thonhauser, P Umari, N Vast, X Wu, and S Baroni. Advanced capabilities for materials modelling with q uantum espresso. *Journal of Physics: Condensed Matter*, 29(46):465901, 2017.

[20] D. R. Cooper, B. D'Anjou, N. Ghattamaneni, B. Harack, M. Hilke, A. Horth, N. Majlis, M. Massicotte, L. Vandsburger, E. Whiteway, and V. Yu. Experimental review of graphene. *ArXiv e-prints*, October 2011.

[21] Katsunori Wakabayashi, Mitsutaka Fujita, Hiroshi Ajiki, and Manfred Sigrist. Electronic and magnetic properties of nanographite ribbons. *Phys. Rev. B*, 59:8271–8282, Mar 1999.